Springer

KSME

Journal of Mechanical Science and Technology 29 (12) (2015) 5281~5288
www.springerlink.com/content/1738-494x(Print)/1976-3824(Online)
DOI 10.1007/s12206-015-1130-x

Three-dimensional wing behaviors of a rhinoceros beetle during takeoff flights †

Boogeon Lee[1], Hyungmin Park[1,2,*] and Sun-Tae Kim[3]

[1]*Department of Mechanical & Aerospace Engineering, Seoul National University, Seoul, 08826, Korea*
[2]*Institute of Advanced Machines and Design, Seoul National University, Seoul, 08826, Korea*
[3]*Agency for Defense Development, Yuseong-gu, Daejeon, 34060, Korea*

(Manuscript Received October 5, 2015; Revised October 31, 2015; Accepted October 31, 2015)

Abstract

We investigated the aerodynamic characteristics of a beetle in a takeoff flight by measuring the temporal and spatial changes in body and wing behaviors. In particular, three-dimensional trajectories and/or deformations of rigid outer wing (elytron) and highly flexible inner wing (hindwing) were measured with three high-speed cameras (at 2000 fps) and reconstructed for the analysis using a modified direct linear transform algorithm. From an inclined rod, the beetle is observed to perform a takeoff flight without the aid of legs, i.e., jumping. Although the elytron is flapped passively induced by the hindwing motion, it is found to have non-negligible flapping amplitude and angle of attack, indicating that the aerodynamic force generation by the elytron itself would be influential. Furthermore, the measured trajectories of an elytron and hindwing imply that the beetle may utilize well-known mechanisms such as a delayed stall, clap-and-fling, wing-wing (elytron-hindwing) interaction, and figure-eight motion. Finally, the flexibility of a hindwing affects the heaving motion (out of the stroke plane) most significantly; i.e., the local variation of the deviation angle along the wing span is more pronounced compared to that of flapping angle and angle of attack.

Keywords: Beetle; Takeoff; Wing kinematics; Flexibility

1. Introduction

The aerodynamic characteristics of insect flight have been investigated vigorously due to the unconventional mechanisms of aerodynamic force generation achieved by sophisticated control of the wing kinematics, and possible transfers to designing small-scale flight vehicles. Quite a few studies have shown that slight changes in unsteady wing trajectories and deformations may cause significant variations in the aerodynamic performance of flapping wings [1-3]. Several mechanisms such as delayed stall, advanced rotation, rotational lift, wake capture, clap and fling, figure-eight motion and wing-wing interaction are now accepted, despite some discrepancies in the details, as causes for a high lift force generation [1-7].

Toward understanding the physics behind insect flights, many different kinds of flying insects such as fruit fly [1, 8, 9], dragonfly [2, 10, 11], hawkmoth [5, 12] and butterfly [6, 13, 14] have been selected as a research target popularly, partly due to relatively easy access to them. On the other hand, the flight of a beetle has received less attention and thus not been studied in detail. A beetle that hides highly flexible inner wings (hereinafter called as hindwings) being folded in a complex manner under the rigid outer wings (elytra) is well known for having the largest wing loading (~35 - 65 N/m^2; ~1 - 3 N/m^2 and ~5 - 10 N/m^2 for a fruit fly and dragonfly, respectively) among flying insects [15], but it has been also observed to effectively perform aerial locomotion. Furthermore, the beetle has characteristic aspects in wing geometry and motions. For example, to initiate a flight, beetles open the elytra and then unfold the hindwings that are actually flapped (i.e., controlled) actively for the flights. Although the beetle does not control the flapping motion of the elytra (rather they are passively moved by the motion of hindwings), the close proximity between elytra and hindwings during the flight indicates that the interaction between them may have an important influence on the aerodynamic performance.

So far, several previous studies have tried to understand the aerodynamics of a beetle flight [16-23]. About the role of elytra associated with flights, for example, de Souza and Alexander [16] claimed that a non-zero dihedral angle of elytra enhances the rolling stability during the flight; however, the direct contribution to aerodynamic force generation is controversial. Johansson et al. [17] have estimated about 40% increase of the lift force based on velocity measurement in the wake behind the elytron, but no significant effects have been reported from the numerical simulations [18, 19]. The wing-

*Corresponding author. Tel.: +82 2 880 4159
E-mail address: hminpark@snu.ac.kr
† Recommended by Associate Editor Kyu Hong Kim

wing interaction between the elytra and hindwings has been also studied. Truong et al. [20], for example, by visualizing the flow around elytra and hindwings using a smoke-wire technique, have explained that the increased suction pressure in the gap between the elytra and hindwings during the upstroke may increase the lift force on hindwings. On the other hand, Le et al. [21] numerically studied that the elytra-hindwings interaction causes an enlarged leading-edge vortex above the elytra, which will increase the lift force generated by elytra. They also claimed that the twisting and camber change of hindwings enhance the aerodynamic performance of a beetle. Kitagawa et al. [22], visualizing the flow around a beetle in a tethered flight with smoke, claimed that the beetle uses the wake capture mechanism to generate the high lift force. The role of horn (only the male beetle has it) also has been investigated and almost no changes of flight performance have been reported [23].

As introduced, less is known for the beetle flight compared to other insect flights, and this is partly due to the limited data available for the wing behavior during flight. That is, detailed measurement and analysis of the wing trajectory and deformation, especially for the highly flexible wings, should be accompanied with understanding the aerodynamic characteristics of flying insects [14, 24-26]. In the literature, there are some data available for describing the motion (or posture) of the elytra and hindwings of a beetle in flights. For the elytra, Frantsevich et al. [27] measured, in a tethered flight condition, that the elytra are positioned to have a negative angle of attack. For the hindwings, it was reported that the flapping frequency is 37 - 40 Hz and 30 - 34 Hz for hovering and forward flights, respectively, while the stroke-plane angle and flapping amplitude are about 10° and 180° for the hovering flight and about 21° and 165° for the forward flight, respectively [19, 28]. Thus, it is understood that a beetle uses a slightly inclined stroke plane and very large flapping amplitude. Truong et al. [29] measured the flapping angle, angle of attack, and body orientation just after a takeoff from the ground. From these previous efforts, some global parameters describing the motion of elytra and/or hindwings are available; however, to perform more detailed investigations (numerical simulations or wind-tunnel experiments with a dynamically-scaled robotic model) of the aerodynamic characteristics of beetle flight, the temporal and spatial (i.e., local) variations of those global parameters due to wing deformation should be understood.

Therefore, we measured and analyzed the three-dimensional deforming behavior of elytra and hindwings, and the body orientations of beetles in flight using three high-speed cameras and modified direct linear transform (MDLT) and visual image correlation algorithms [25, 30]. Among different flight modes, we focused on the takeoff flight because it requires the largest force generation to lift the body, which is a good starting point to investigate the aerodynamics of beetle flight [29, 31]. We believe this will be a good reference to initiate a more in-depth study of the beetle aerodynamics.

Table 1. Morphological parameters of the beetles whose takeoff flights are filmed.

Beetle individual		B1	B2
Body mass, m [g]		5.9	5.7
Elytron	span, S_e [mm]	32.2	32.6
	chord, c_e [mm]	16.9	17.2
	area, A_e [mm^2]	450.7	459.6
	aspect ratio, AR_e	2.30	2.31
Hindwing	span, S_h [mm]	51.6	51.6
	chord, c_h [mm]	15.9	19.6
	area, A_h [mm^2]	688.9	794.6
	aspect ratio, AR_h	3.96	3.35
Hindwing tip-to-tip distance, L [mm]		109.7	111.4

2. Experimental setup and procedure

2.1 Tested beetles

We prepared about 20 rhinoceros beetles, which were purchased from a commercial insect distributor in Korea and reared in an acrylic cage of which the inside is decorated with soils, leaves and branches. While observing the behavior of the beetles, we tried to find a way to make the beetle initiate a takeoff flight, without putting unnecessary stresses on the insects. After testing several ways advised by the distributor or a previous study [29], we found that when a beetle is placed on an inclined wooden rod, mimicking the branch of a tree, it tends to crawl upward and takeoff at the tip of the rod. With this approach, it is possible to film the takeoff flights of the beetle successively under the same condition (i.e., it is confirmed that the measured wing kinematics are repeatable as shown below).

After the time-resolved sequences of takeoff flight were taken successfully, we measured the morphological parameters of the same individual beetle. As commented previously [27, 29], in general, female beetles show a better flight tendency than males, and thus active female beetles were chosen for measurements. As a result, we were able to analyze the five takeoff flights from the rod, which were performed by two different individuals. The morphometric parameters are summarized in Table 1. Here, the chord length denotes the maximum chord of the wing and the aspect ratio (AR) is defined as $AR = S^2/A$. As shown in the table, beetles in the present study have a body mass about 6 g, while the size of hindwing is larger than the elytron. For the tested beetles, the hindwings have an averaged AR of about 3.3 - 3.9, which is larger than that (about 2.3) of elytra.

2.2 Tracking of three-dimensional wing behaviors

To measure the three-dimensional wing motions and deformations, we used three high-speed cameras and two 2 kW-Tungsten portable lights as an illumination source, distributed around a customized studio frame (2.0 m × 2.0 m × 2.0 m)

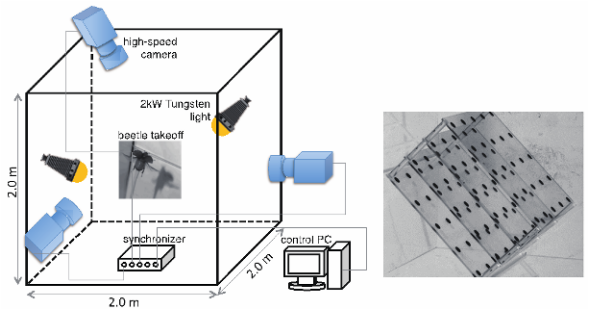

(a) (b)

Fig. 1. (a) Experimental setup for recording three-dimensional wing kinematics of a beetle in takeoff flights using three high-speed cameras and two tungsten lights; (b) three dimensional calibration target with one hundred markers.

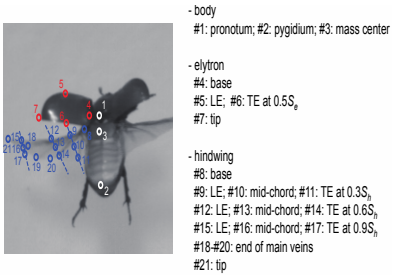

Fig. 2. Distribution of twenty-one morphological markers to track the three-dimensional behavior of the body, elytron and hindwing of a beetle.

that is covered with blackout curtains to block any external disturbances during the experiments (Fig. 1(a)). Three high-speed cameras, one located on the top and two capturing side views, were operated simultaneously via a synchronizer. The image capturing was done for about 1.5 seconds at the rate of 2000 fps with a spatial resolution of 512 × 512 pixels. Considering the typical flapping frequency of a beetle hindwing (30 - 40 Hz), this condition is enough to measure several wing beats to be analyzed. To calibrate the cameras, we used an in-house calibration target (Fig. 1(b)) that has 100 circular dots distributed with a spacing of 40 mm in lateral and vertical directions. With three cameras in position, the error in tracking markers is less than 1%.

To track specific points on the wing, it is necessary to mark the position to be detected. Instead of using hard markers (e.g., thin metal film or small paint drop) [26, 27], we used soft markers that are morphologically discernible features to make beetles fly without external disturbances. As shown in Fig. 2, we selected twenty-one morphological markers located on an elytron, hindwing and body of a beetle. That is, three are on the body (#1: pronotum, #2: pygidium, #3: mass center), four are on the elytron (#4: base, #5: leading edge at the mid-span, #6: trailing edge at the mid-span, #7: tip) and fourteen positions (#8: base, #9-#11: leading edge, mid-chord and trailing edge at 0.3S_h, #12-#14: leading edge, mid-chord and trailing edge at 0.6S_h, #15-#17: leading edge, mid-chord and trailing edge at 0.9S_h, #18-#20: end of main veins, #21: tip) are distributed on the hindwing. Without using hard markers, it is possible to track each morphological marker by visual image correlation method [25, 30].

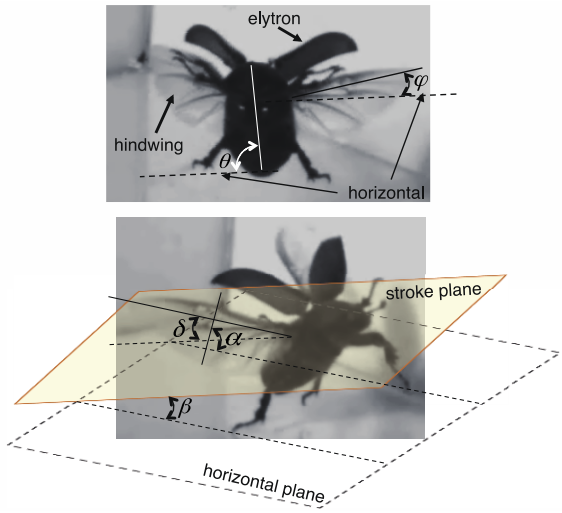

Fig. 3. Definitions of the parameters describing the wing kinematics of a flying beetle, shown for the hindwing and same definitions are applied to the elytron.

Among several techniques developed for the re-construction of three-dimensional wing kinematics, in the present study, we used Modified direct linear transform (MDLT) algorithm with visual image correlation method. According to Direct linear transform (DLT) algorithm, three-dimensional position vectors in real world (***A***) and image plane (***B***) should satisfy the simple linear correlation of $\boldsymbol{B} = c\boldsymbol{A}$ (***c***: scaling factor), which is called as a collinearity condition [32]. While getting the relation between the coordinates in real and image planes, we needed to determine eleven DLT coefficients, but only ten independent parameters were available with the collinearity condition only. To solve this problem, Hatze [30] suggested to consider a non-linear constraint additionally, which is called as Modified direct linear transform (MDLT) algorithm. On the other hand, to track the specific points (designated based on the morphological features) on the wing, the cross-correlation of pixels was performed across the acquired image sequences, called as visual image correlation method [25, 30]. For the details about the tracking methods, please refer to Ref. [25].

2.3 Definitions of wing-kinematic parameters

Fig. 3 defines the wing-kinematic parameters that are to be calculated from the measured wing behaviors. Body angle (θ) is the angle between the horizontal and the line connecting pronotum and pygidium. Stroke-plane angle (β) is defined as the angle between the stroke plane and the horizontal plane. Flapping angle (φ) and angle of attack (α) are defined as the angle between the line joining the wing base and tip and its projection onto the horizontal plane and the angle between the local wing chord and the horizontal plane, respectively. On the other hand, the deviation angle (δ) is defined as the angle be-

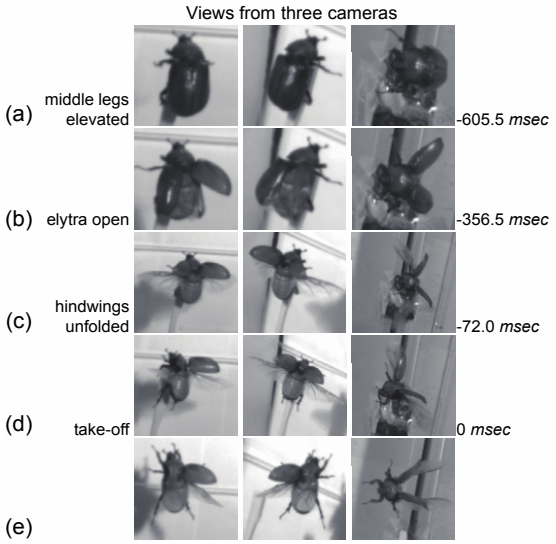

Fig. 4. Typical sequence of a beetle takeoff from an inclined rod, measured at 2000 fps.

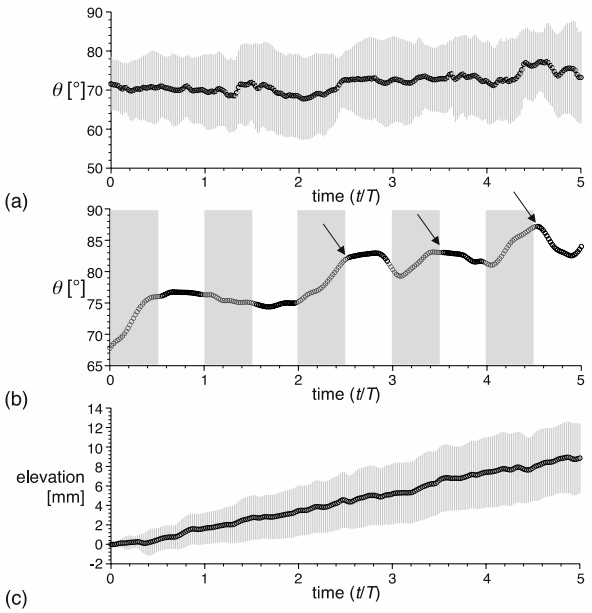

Fig. 5. Temporal variations in body angle (θ) (a, b) and elevation of mass center (c) during takeoff flights. For the body angle, the averaged data (a) and a representative single data set (b) are shown separately. In (a) and (c), symbols and lines denote the averaged value and accompanied deviations, respectively. Here, T is the period of flapping hindwing and shaded area denote the stage of up-stroke.

tween the line joining the wing base and tip and its projection onto the stroke plane. For all the parameters, the subscript of '*e*' and '*h*' denote the elytron and hindwing, respectively.

3. Results and discussion

3.1 Sequential description of a takeoff flight

Typical behavioral sequence of takeoff flights from an inclined rod is shown in Fig. 4. The time separation between each major events identified may change slightly depending on each trial, but the sequence in Fig. 4 was observed commonly for all the tests performed in the present study. As shown, the beetle raises its middle legs first (at t = -605.5 msec, Fig. 4(a)) and then opens its elytra (at t = -356.5 msec, Fig. 4(b)). After the elytra are fully opened, the beetle unfolds the hindwings (at t = -72.0 msec, Fig. 4(c)) and initiates flapping hindwings. The beetle is completely detached from the rod (at t = 0 msec, Fig. 4(d)) within one to two wing beats with fully stretched hindwings, and we measured and analyzed the first five wing beats for each trial. After the takeoff, the beetle performs various flight modes such as hovering, forward and turning flights. In the present cases, we did not observe any hints about the jumping-assisted takeoff flight, which was also reported by Truong et al. [29] who measured the beetle takeoff flight from a flat ground. The time separations between major events for the takeoff flight in Fig. 4 are also in a similar range with that of Truong et al. [29]. Although Truong et al. [29] observed the change in the order between middle-leg elevation and elytra opening in some cases, in the present cases the middle-leg elevation always precedes the elytra opening.

3.2 Body orientation

In this section, the body orientation of a beetle during a takeoff is discussed. Figs. 5(a) and (b) show the temporal variations of averaged and single data set of body angle (θ), respectively. For the rod takeoff, the beetle takes a very large averaged body angle (about 70°) (Fig. 5(a)). This is different from the takeoff from the ground where the body angle gradually increases as the beetle rises [29]. Although the averaged body angle does not show specific trend on the wing motion, for a single data it is clearly observed that the body angle oscillates in relation to the wing motion. As shown in Fig. 5(b), after the first two strokes of hindwing, i.e., once the beetle is completely off the rod for the takeoff, the body angle increases (decreases) during the stage of up-stroke (down-stroke) of the hindwing and thus has a peak at the end of an up-stroke (denoted as arrows in Fig. 5(b)). Similar trend has been reported for the ground takeoff as well [29]. On the other hand, the comparison of averaged body angle (Fig. 5(a)) and a single data (Fig. 5(b)) indicates that one needs to be very careful in representing the kinematic parameters measured with living creatures, by which some important characteristics may be buried by averaging the data with large scatters and different time constants.

Fig. 5(c) shows the elevation (i.e., vertical translation) of the center of mass during the takeoff. Here, the center of mass (maker #3) is approximately determined by searching the point that makes the beetle suspended with a string balanced with a horizontal. After testing several different individuals, it was found that the center of mass is located at about 45 - 50% of the body length. Again the symbols show the averaged values from repeated trials, and the lines show the range of

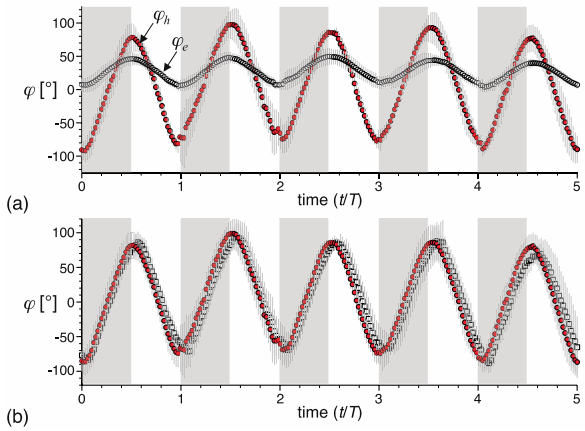

Fig. 6. (a) Time history of flapping angles (φ) of elytron (○) and hindwing (●) for the takeoffs from an inclined rod. Here, φ's are determined by the movement of wing tips. (b) Comparison of φ of a hindwing based on the movement of wing tip (●) and leading-edge at $0.6S_h$ (□, marker #12). Here, T is the period of flapping hindwing and shaded area denote the stage of up-stroke. Symbols and lines denote the averaged value and accompanied deviations, respectively.

data scatters. As time goes on, the elevation increases gradually showing that the beetle actually takes off the rod for flight. Unlike the body angle, the elevation for a single data set shows the same trend with the averaged one (not shown here).

3.3 Global wing-kinematic parameters

For the present takeoff flights from an inclined rod, the flapping frequency of a hindwing is measured to be 39.6 Hz (± 0.7 Hz), which is in a similar range with previous measurements (38 - 42 Hz) [29]. Although it is not controlled actively, the elytron also shows a periodic motion induced by the flapping hindwing (see Fig. 6) and its frequency is about 38.1 Hz (± 0.9 Hz).

Another global parameter to characterize the wing motion is a stroke-plane angle (Fig. 3). For the rod takeoff, it is measured that the stroke-plane angles of elytron and hindwing are 18.6° (± 4.1°) and 16.5° (± 5.7°), respectively. Thus, the beetle utilizes a slightly inclined stroke plane, compared to the horizontal stroke plane of a fruit fly ($\beta \sim 0°$) and the highly inclined stroke plane of a dragonfly ($\beta \sim 60°$). Thus, it is assumed that the contribution of lift force to the vertical force generation to takeoff is larger than that from the drag force. Interestingly, the elytron also has a similar stroke-plane angle to the hindwing, which indicates that the elytra itself may not incur a significant aerodynamic cost due to the drag force acting on it.

3.4 Temporal variation in wing trajectory

Fig. 6(a) shows the time history of flapping angles (φ) of elytron and hindwing for the first five strokes during takeoff. Here, the flapping angle is calculated based on the movement of wing tips (markers #7 and #21). In the figure, symbols denote the averaged values with the lines for the range of deviation. While the periodic motions of elytron and hindwing are well captured (approximately following a sinusoidal function), the flapping amplitudes (Φ) of elytron and hindwing are 38.8° (± 4.2°) and 164.2° (± 7.3°), respectively. Since the elytron undulates passively, the flapping angle of the elytron shows a slight phase difference from that of the hindwing; however, it is interesting that the elytron also has non-negligible flapping amplitude as well. Although it is much smaller than that of a hindwing, considering that the flapping frequency of elytron is comparable to that of a hindwing, this implies that the elytron itself would produce aerodynamic forces that affect the overall aerodynamic performance of a beetle [17]. On the other hand, the fairly large flapping amplitude and deflection (i.e., deformation) of the hindwing suggest that the clap-and-fling mechanism [4] may work during the stroke reversal to enhance the aerodynamic performance as well. As previous studies have suggested, the wing-wing interaction caused by the close proximity between the elytra and hindwing can affect the aerodynamic performance. As shown in the temporal variation of flapping angle, this interaction may happen during the transition from up-stroke to down-stroke when the gap between elytron and hindwing becomes the smallest.

To see the influence of wing deformation, the flapping angles of a hindwing based on the movement of inner wing positions (leading edge at $0.6S_h$) are additionally calculated for a comparison. Note that the elytron does not experience a discernible deformation during flapping. As shown in Fig. 6(b), almost the same flapping amplitude is maintained along the spanwise direction, but the phase difference increases from the wing tip to base. Also, the range of deviation between each data set is the largest at the wing tip, while it is the smallest near the wing base, indicating that the amount of deformation differs locally, which is the largest near the wing tip. Since the spanwise flow over the wing has been one of the mechanisms to induce the leading-edge vortices to be attached on a flapping insect wing, which results in the delayed stall, the most commonly proposed mechanism of large aerodynamic force generation among different flying insects [1-3, 5-11], this spanwise deformation of the hindwing with a phase difference would affect the dynamics of the leading-edge vortices.

Next, the variations of angle of attack (α) are discussed. Fig. 7(a) shows the time history of averaged angle of attack for elytron (α_e) and hindwing (α_h), measured based on the mid-chord ($0.5S_e$) and chord-line at $0.6S_h$, respectively. Overall, the elytron and hindwing have almost constant angles of attack during up- and down-strokes, respectively, while the angle of attack during the up-stroke (α_u) is larger than that during the down-stroke (α_d). For the elytron, α_u = 99.9° (± 19.5°) and α_d = 72.5° (± 12.6°) and the hindwing has α_u = 133.3° (± 24.3°) and α_d = 45.3° (± 23.0°). Large angles of attack during up- and down-strokes show that the beetle also utilizes the massively separated flow at the leading edge of the wing as a major source for the aerodynamic force generation. For both, elytron and hindwing, the durations of pronation and supina-

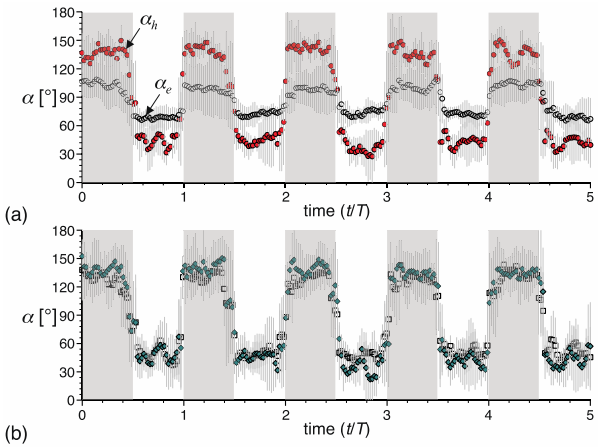

Fig. 7. (a) Time history of attack angles (α) of elytron (○) and hindwing (●) for the takeoffs from an inclined rod. Here, α's are determined at the spanwise positions of $0.5S_e$ (elytron) and $0.6S_h$ (hindwing). (b) Comparison of α of a hindwing at the spanwise positions of $0.3S_h$ (□) and $0.9S_h$ (◆). Here, T is the period of flapping hindwing and shaded area denote the stage of upstroke. Symbols and lines denote the averaged value and accompanied deviations, respectively.

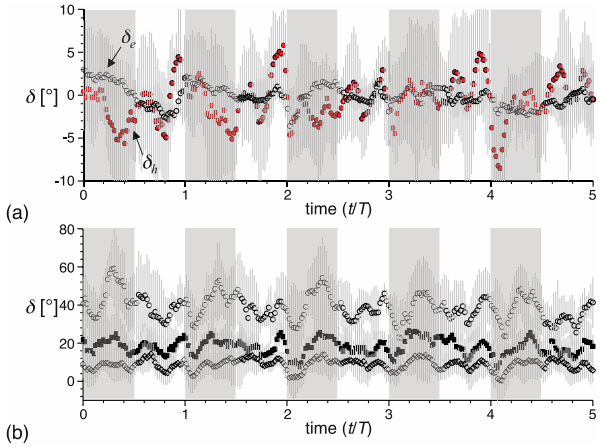

Fig. 8. (a) Time history of deviation angles (δ) of elytron (○) and hindwing (●) for the takeoffs from an inclined rod. Here, δ's are determined by the movement of wing tips. (b) Comparison of δ's measured based on the movements of trailing-edge at $0.3S_h$ (○, marker #11), $0.6S_h$ (■, marker #14) and $0.9S_h$ (◇ , marker #17).

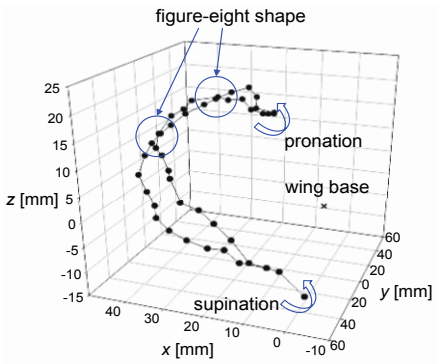

Fig. 9. Three-dimensional view for the figure-eight movement of a hindwing tip during the second stroke in takeoff from an inclined rod.

tion were approximately equal and are achieved very fast (takes about 22% of the one stroke period for the rotation of the hindwing). Therefore, the hindwing should rotate at a rate of 1.1 rad/msec, indicating that the contribution of rotational lift during the stroke reversal should be important as well. Although the amplitude of wing rotation of elytron is relatively smaller than that of a hindwing, the fact that the elytron also has a fairly large angle of attack during flapping again indicates that the aerodynamic forces generated by the elytron itself would not be trivial [17].

Fig. 7(b) shows the variation of the angle of attack on a hindwing, measured based on the chord-line of 30% and 90% of the wingspan (S_h). While they show similar trends to that of the angle of attack measured at $0.6S_h$ (Fig. 7(a)), it is measured that α_u = 125.8° (± 26.1°) and α_d = 51.7° (± 20.2°) at $0.3S_h$, and α_u = 133.6° (± 26.9°) and α_d = 45.9° (± 27.2°) at $0.9S_h$. Therefore, the effect of local incidence angle of the flow along the spanwise direction would not be significant.

Finally, the time history of averaged deviation angle (δ), representing the wing motions out of the stroke plane (it is noted that the stroke plane is defined as the movement of wing tip), is plotted for the elytron and hindwing, based on the movement of wing tips (makers #7 and #21) (Fig. 8(a)). Instead of showing specific trends depending on up- and downstrokes, the averaged deviation angle varies less in a relatively narrower range and δ_h is larger than δ_e. When the single data set is traced, interestingly, it is clearly seen that the wing tip of the beetle hindwing moves following the figure-eight motion of wing tip, which is well known as a common wing behavior in flying insects to enhance the aerodynamic force generation [2]. During the first and second strokes for the takeoff, double-figure-eight motion is measured (Fig. 9), which changes to a single-figure-eight motion after third strokes. From this, it is found that the beetle also utilizes a similar mechanism to enhance the aerodynamic performance. At the inner wing positions, on the other hand, the deviation angle increases significantly toward the wing base (Fig. 8(b)). Among flapping angle, angle of attack, and deviation angle, the rate of local variation along the spanwise direction due to deformation is the largest for the deviation angle. Therefore, it is thought that it is important to investigate the effect of the heaving motion of the hindwing to understand how the wing flexibility affects the aerodynamic performance of a beetle.

In the present study, we measured the beetle takeoff flight from an inclined rod which a previous study by Truong et al. [29] had measured the takeoff from flat ground. In Fig. 10, the temporal variations of flapping and attack angles are compared. As shown, during the first and second strokes, there is a slight difference, but after the third stroke, they agree well with each other. This is because Truong et al. [29] measured the wing motion after the beetle clear off the ground, i.e., when the ground does not interfere with the hindwing motion. However, in the present study, the first and second strokes of

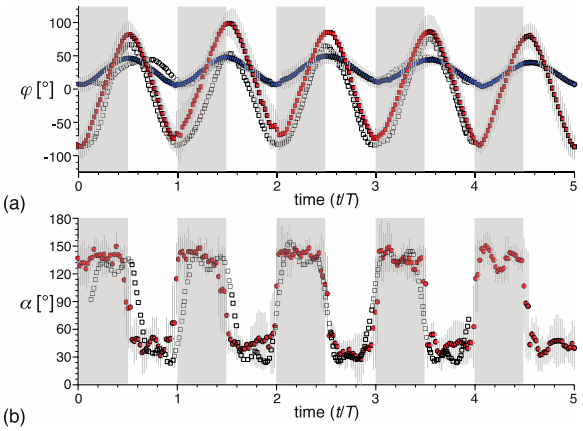

Fig. 10. Comparison of flapping angles (a) and angle of attacks (b) between the present measurement and those from Truong et al. [29]: (a) ●, φ_e (present); ○, φ_e [29]; ■, φ_h (present); □, φ_h [29]; (b) ●, α_h (present); ○, α_h [29]. Here, T is the period of flapping hindwing and shaded area denote the stage of upstroke. Symbols and lines denote the averaged value and accompanied deviations, respectively.

the hindwing are performed when the movement of a beetle is still in the interaction with the rod. Therefore, the wing motion itself is not affected by the location from which the beetle takes off, once it is cleared off the rod or ground. However, it is further necessary to measure the wing motions when the ground actually interferes with it, in order to investigate the differences between the takeoff from a rod and ground in detail.

4. Concluding remarks

We have measured the three-dimensional behaviors of the body and wings (elytron and hindwing) of a beetle during its takeoff from an inclined rod using three high-speed cameras. Employing a modified direct linear transform algorithm, temporal and spatial variations of the wing movement have been analyzed in terms of the major parameters for the wing-beat kinematics. It is found that the elytron, which is flapped passively due to the movement of a hindwing, has non-negligible flapping amplitude and angle of attack, indicating that the elytron itself would contribute to the aerodynamic force generation. Furthermore, from the measured trajectories of elytron and hindwing, many hints are evidenced implying that the beetle may utilize well-known mechanisms for unconventional aerodynamic force generation, such as a delayed stall with an attached leading-edge vortex, clap-and-fling, wing-wing interaction, and figure-eight motion. It would be interesting to examine whether the beetle actually uses these mechanisms during the flight. Finally, the wing flexibility affects the heaving motion (i.e., out-of-stroke-plane motion) most significantly compared to the local variations of flapping angle and angle of attack along the wing span. We think the present study is a good reference to initiate an in-depth investigation of the beetle aerodynamics (via wind-tunnel experiments or numerical simulation), focusing on the mechanism of regulating aerodynamic performance and possible ground effect during takeoff from the ground.

Acknowledgment

This research was supported by a grant to Bio-Mimetic Robot Research Center Funded by Defense Acquisition Program Administration, and by Agency for Defense Development (UD130070ID).

Nomenclature

A	: Wing planform area
AR	: Wing aspect ratio (= S^2/A)
c	: Chord length, mm
L	: Distance between tip to tip, mm
m	: Body mass, kg
S	: Wing span, mm
α	: Angle of attack
α_d	: Angle of attack during a down-stroke
α_u	: Angle of attack during an up-stroke
β	: Stroke-plane angle
δ	: Deviation angle
θ	: Body angle
φ	: Flapping angle
Φ	: Amplitude of the flapping angle

References

[1] M. H. Dickinson, F. O. Lehmann and S. P. Sane, Wing rotation and the aerodynamic basis of insect flight, *Science*, 284 (1999) 1954-1960.

[2] Z. J. Wang, Dissecting insect flight, *Annu. Rev. Fluid Mech.*, 37 (2005) 183-210.

[3] W. Shyy, Y. Lian, J. Tang and H. Liu, *Aerodynamics of low reynolds number flyer*, Cambridge University Press, New York, USA (2008).

[4] T. Weis-Fogh, Quick estimates of flight fitness in hovering animals, including novel mechanisms for lift production, *J. Exp. Biol.*, 59 (1973) 169-230.

[5] C. P. Ellington, C. Van den Berg, A. P. Willmott and A. L. R. Thomas, Leading-edge vortices in insect flight, *Nature*, 384 (1996) 626-630.

[6] R. B. Srygley and A. L. R. Thomas, Unconventional lift-generating mechanisms in free-flying butterflies, *Nature*, 420 (2002) 660-664.

[7] F. O. Lehmann and S. Pick, The aerodynamic benefit of wing-wing interaction depends on stroke trajectory in flapping insect wings, *J. Exp. Biol.*, 2010 (2007) 1362-1377.

[8] M. Sun and J. Tang, Unsteady aerodynamic force generation by a model fruit fly wing in flapping motion, *J. Exp. Biol.*, 205 (2002) 55-70.

[9] J. Kweon and H. Choi, Sectional lift coefficient of a flapping wing in hovering motion, *Phys. Fluids*, 22 (2010) 075106.

[10] A. L. R. Thomas, G. K. Taylor, R. B. Srygley, R. L. Nudds

and R. J. Bomphrey, Dragonfly flight: free-flight and tethered flow visualizations reveal a diverse array of unsteady lift-generating mechanisms, controlled primarily via angle of attack, *J. Exp. Biol*., 207 (2004) 4299-4323.

[11] H. Park and H. Choi, Kinematic control of aerodynamic forces on an inclined flapping wing with asymmetric strokes, *Bioinspir. Biomim*., 7 (2012) 016008.

[12] L. Zhao and X. Deng, Power distribution in the hovering flight of the hawk moth, *Manduca sexta*, *Bioinspir. Biomim*., 4 (2009) 046003.

[13] A. Chakravarthy and R. Albertani, Experimental kinematics and dynamics of butterflies in natural flight, *AIAA Paper 2009-873* (2009).

[14] Y. I. Jang and S. J. Lee, Dynamic motion of a butterfly *Argyronome laodice* in ground take-off flight, *J. Mech. Sci. Tech*., 6 (2013) 1763-1769.

[15] N. S. Ha, Q. T. Truong, N. S. Goo and H. C. Park, Relationship between wingbeat frequency and resonant frequency of the wing in insects, *Bioinspir. Biomim*., 8 (2013) 046008.

[16] M. M. de Souza and D. E. Alexander, Passive aerodynamic stabilization by beetle elytra (wing covers), *Physiol. Entomol*., 22 (1997) 109-115.

[17] L. C. Johansson, S. Engel, E. Baird, M. Dacke, F. T. Muijres and A. Hedenstrom, Elytra boost lift, but reduce aerodynamic efficiency in flying beetles, *J. R. Soc. Interface*, 9 (2012) 2745-2748.

[18] P. E. Sitorus, H. C. Park, D. Byun, N. S. Goo and C. H. Han, The role of elytra in beetle flight: I. generation of quasi-static aerodynamic forces, *J. Bionic Eng*., 7 (2010) 354-363.

[19] T. Q. Le, D. Byun, Saputra, J. H. Ko, H. C. Park and M. Kim, Numerical investigation of the aerodynamic characteristics of a hovering Coleopteran insect, *J. Theo. Biol*., 266 (2010) 485-495.

[20] T. V. Truong, T. Q. Le, H. T. Tran, H. C. Park, K. J. Yoon and D. Byun, Flow visualization of rhinoceros beetle (*Trypoxylus dichotomus*) in free flight, *J. Bionic Eng*., 9 (2012) 304-314.

[21] T. Q. Le, T. V. Truong, S. H. Park, T. Q. Truong, J. H. Ko, H. C. Park and D. Byun, Improvement of the aerodynamic performance by wing flexibility and elytra-hind wing interaction of a beetle during forward flight, *J. R. Soc. Interface*, 10 (2013) 20130312.

[22] K. Kitagawa, M. Sakakibaraand and M. Yasuhara, 2009, Visualization of flapping wing of the drone beetle, *J. Visualization*, 12 (2009) 393-400.

[23] E. L. McCullough and B. W. Tobalske, Elaborate horns in a giant rhinoceros beetle incur negligible aerodynamic costs, *Proc. R Soc. B*, 280 (2013) 20130197.

[24] H. Wang, L. Zeng, H. Liu and C. Yin, Measuring wing kinematics, flight trajectory and body attitude during forward flight and turning maneuvers in dragonflies, *J. Exp. Biol*., 206 (2003) 745-757.

[25] T. Hedrick, Software techniques for two- and three-dimensional kinematic measurements of biological and biomimetic systems, *Bioinspir. Biomim*., 3 (2008) 034001.

[26] C. Koehler, Z. Liang, Z. Gaston, H. Wan and H. Dong, 3D reconstruction and analysis of wing deformation in free-flying dragonflies, *J. Exp. Biol*., 215 (2012) 3018-3027.

[27] L. Frantsevich, Z. Dai, W. Y. Wang and Y. Zhang, Geometry of elytra opening and closing in some beetles (*Coleoptera, Polyphaga*), *J. Exp. Biol*., 208 (2005) 3145-3158.

[28] Q. V. Nguyen, H. C. Park, N. S. Goo and D. Byun, Characteristics of a beetle's free flight and a flapping-wing system that mimics beetle flight, *J. Bionic Eng*., 7 (2010) 77-86.

[29] T. V. Truong, T. Q. Le, H. C. Park, K. J. Yoon, M. J. Kim and D. Byun, Non-jumping take off performance in beetle flight (Rhinoceros Beetle *Trypoxylus dichotomus*), *J. Bionic Eng*., 11 (2014) 61-71.

[30] H. Hatze, High-precision three-dimensional photogrammetric calibration and object space reconstruction using a modified DLT-approach, *J. Biomech*., 21 (1988) 533-538.

[31] J. H. Marden, Maximum lift production during takeoff in flying animals, *J. Exp. Biol*., 130 (1987) 235-258.

[32] G. A. Wood and R. N. Marshall, The accuracy of DLT extrapolation in three-dimensional film analysis. *J. Biomech*., 19 (1986) 781-783.

Boogeon Lee received his B.S. in Mechanical Engineering from Hanyang University, Seoul, Korea, in 2014. He is currently working toward his Ph.D. at the Multiphase Flow & Flow Visualization laboratory, Department of the Mechanical and Aerospace Engineering, Seoul National University. His current research areas are insect flight and fluid-structure interaction.

Hyungmin Park obtained his B.S. and Ph.D. at the Department of Mechanical & Aerospace Engineering, Seoul National University, Korea, in 2000 and 2010, respectively. Dr. Park is currently an assistant professor there. His research interests include multiphase flow, flow control with superhydrophobic surfaces, and fluid-structure interaction.

Sun-Tae Kim obtained his B.S. and Ph.D. at the Department of Aeronautical & Aerospace Engineering, Seoul National University, Korea, in 1993 and 1996, respectively. He is currently a Principal Researcher at the Aerodynamics Division, Agency of Defense Development. His research interests include aerodynamic analysis for the vertical flow over delta wing, the ground effects of airplane, and the cavity flow.